

The power of relativistic jets is larger than the luminosity of their accretion disks

G. Ghisellini¹, F. Tavecchio¹, L. Maraschi², A. Celotti^{1,3,4}, T. Sbarrato^{1,5,6}

1. INAF – Osservatorio Astronomico di Brera, via E. Bianchi 46, I-23807, Merate, Italy
2. INAF – Osservatorio Astronomico di Brera, via E. Brera 28, I-20121, Milano, Italy
3. SISSA, Via Bonomea 265, I-34135, Trieste, Italy
4. INFN–Sezione di Trieste, via Valerio 2, I-34127 Trieste, Italy
5. Univ. dell’Insubria, Dipartimento di Fisica e Matematica, Via Valleggio 11, I-22100 Como, Italy
6. ESO–European Southern Observ., Karl–Schwarzschild–Strasse 2, 8578 Garching bei München, Germany

Theoretical models for the production of relativistic jets from active galactic nuclei predict that jet power arises from the spin and mass of the central black hole, as well as the magnetic field near the event horizon¹. The physical mechanism underlying the contribution from the magnetic field is the torque exerted on the rotating black hole by the field amplified by the accreting material. If the squared magnetic field is proportional to the accretion rate, then there will be a correlation between jet power and accretion luminosity. There is evidence for such a correlation^{2–8}, but inadequate knowledge of the accretion luminosity of the limited and inhomogeneous used samples prevented a firm conclusion. Here we report an analysis of archival observations of a sample of blazars (quasars whose jets point towards Earth) that overcomes previous limitations. We find a clear correlation between jet power as measured through the γ –ray luminosity, and accretion luminosity as measured by the broad emission lines, with the jet power dominating over the disk luminosity, in agreement with numerical simulations⁹. This implies that the magnetic field threading the black hole horizon reaches the maximum value sustainable by the accreting matter¹⁰.

The jet power is predicted¹ to depend on $(aMB)^2$, where a and M are respectively the spin and mass of the black hole and B is the magnetic field at its horizon. Seed magnetic fields are amplified by the accretion disk up to equipartition with the mass energy density $\sim \rho c^2$ of the matter accreting at the rate \dot{M} . A greater \dot{M} implies a larger ρ , that can sustain a larger magnetic field, which in turn can tap a larger amount of the black hole rotational energy. The magnetic field is thus a *catalyst* for the process. Increasing the spin of the black hole shrinks the innermost stable orbit, increasing the accretion efficiency η (defined by $\eta = L_{\text{disk}}/\dot{M}c^2$) (L_{disk} accretion disk luminosity) to a maximum value¹¹ $\eta = 0.3$.

We use a well designed sample of blazars that have been detected in the γ –ray band by the *Fermi* Large Area Telescope (LAT) that have been spectroscopically observed in the optical^{12,13} (see Methods). They have been classified as BL Lac objects or Flat Spectrum Radio Quasars (FSRQs) according if the rest frame equivalent width of their broad emission lines was greater (FSRQ) or smaller (BL Lacs) than 5 Å (rest frame). The sample contains 229 FSRQs, and 475 BL Lacs. Of the latter, 209 have a spectroscopically measured redshift. We considered all FSRQs with enough multi–wavelength data to have a Spectral Energy Distribution (SED) that allows to establish the bolometric luminosity. The considered FSRQs amount to 191 objects. Instead, for BL Lacs, we consider only the 26 sources with detected broad emission lines. This makes them the low disk luminosity tail of of the full

blazar sample. This choice is dictated by our will to measure the accretion luminosity, together with the jet power. Through the visible broad emission lines we reconstruct, through a template^{14,15}, the luminosity of the entire broad line region. The latter is a proxy of the accretion disk luminosity, $L_{\text{BLR}} = \phi L_{\text{disk}}$, with¹⁶ $\phi \sim 0.1$. This disk luminosity L_{disk} is then directly given by the observed broad emission lines, avoiding the contamination by the non-thermal continuum. Uncertainties are admittedly large (factor ~ 2) for specific sources, but the averages should be representative of the true values.

To model the non-thermal jet emission, we applied to all objects a simple one-zone leptonic model¹⁷ (see Methods), from which we derive the physical parameters of the jet. The only parameter of interest here, however, is the bulk Lorentz factor Γ of the outflowing plasma, found in the range 10–15 (see Methods and Extended Data Fig. 2). This range is similar to that obtained via measurements of the superluminal motion of the radio components, which however occurs on larger distances from the black hole. The bulk Lorentz factor is thus only weakly model-dependent. Having the bolometric jet luminosity $L_{\text{jet}}^{\text{bol}}$ and Γ , the power that the jet spent in producing the non thermal radiation is¹⁸:

$$P_{\text{rad}} = 2f \frac{L_{\text{jet}}^{\text{bol}}}{\Gamma^2} \quad (1)$$

where the factor 2 accounts for two jets and f , of order unity, is discussed in the Methods section. If this were the entire power of the jet, it would be entirely spent to produce the observed radiation. The jet would stop, and could not produce the radio lobes and/or the extended radio emission we see from these objects. It is then a strict *lower limit* of the jet power.

Fig. 1 shows P_{rad} as a function of L_{disk} for all the 217 considered blazars. There is a robust correlation between the two: $\log P_{\text{rad}} = 0.98 \log L_{\text{disk}} + 0.639$ (with a probability $P < 10^{-8}$ to be random, even taking into account the common redshift dependence). We thus find a linear correlation between the minimum jet power and the accretion luminosity, as expected. Moreover, the two are of same order. This holds also for the considered BL Lacs that do show broad emission lines. The dispersion along the fitting line is $\sigma = 0.5$ dex. An important contribution to this dispersion comes from the large amplitude variability of the non-thermal flux displayed by all blazars, especially in the γ -ray band, where the bolometric jet luminosity peaks. This is true even if we considered the LAT luminosity averaged over two years¹⁹, as shown by the comparison between LAT and older Energetic Gamma Ray Experiment Telescope (EGRET, onboard the *Gamma Ray Compton Observatory*) results: about 20% of the EGRET detected blazars are not detected by LAT²⁰, even though the latter has a 20-fold better sensitivity.

The power in radiation P_{rad} is believed to be about 10% of the jet power P_{jet} and, remarkably, this holds true both for Active Galactic Nuclei (AGN) and Gamma-Ray Bursts²¹. We confirm this result, if there is one proton per emitting lepton (see Methods and Extended data Figure 1). This limits the importance of electron-positron pairs, that would reduce the total jet power. In addition, pairs cannot largely outnumber protons, since otherwise the Compton rocket effect would stop the jet¹⁸ (see Methods).

An inevitable consequence of $P_{\text{jet}} \sim 10P_{\text{rad}}$ is that the jet power is larger than the disk luminosity. Therefore the process that launches and accelerates jets must be extremely efficient, and might be the *most* efficient way of transporting energy from the vicinity of the black hole to infinity.

Assuming $\eta = 0.3$, appropriate for fastly rotating black holes, we have $\dot{M}c^2 = L_{\text{disk}}/\eta$. Fig. 2 shows the jet power P_{jet} vs $\dot{M}c^2$ for all our sources. The white stripe indicates equality. The black line is the best fit correlation [$\log P_{\text{jet}} = 0.92 \log(\dot{M}c^2) + 4.09$] and lies always above the equality line. This finding is fully consistent with recent general relativistic magnetohydrodynamic numerical simulations⁹, in which the average outflowing power in jets and winds reaches 140% of $\dot{M}c^2$ for dimensionless spin values $a = 0.99$. The presence of the jet implies that the gravitational potential energy of the falling matter can not only be transformed into heat and radiation, but can also amplify the magnetic field, allowing the field to access the large store of black hole rotational energy and transform part of it into jet mechanical power. This jet power is somewhat larger than the entire gravitational power $\dot{M}c^2$ of the accreting matter. This is not a coincidence, but the result of the catalyst role of the magnetic field amplified by the disk. When the magnetic energy density exceeds the energy density $\sim \rho c^2$ of the accreting matter in the vicinity of the last stable orbit, the accretion is halted and the magnetic energy decreases, as shown by numerical simulations^{9,22}, and confirmed by recent observational evidence¹⁰.

The mass of the black holes of the FSRQs in our sample has been calculated¹² assuming that the size of the broad line region scales with the square root of the ionizing disk luminosity as indicated by reverberation mapping^{23,24}, and by assuming that the clouds producing the broad emission lines are virialized. The uncertainties associated to this method are large (dispersion of $\sigma = 0.5$ dex for the black hole mass values²⁵), but if there is no systematic error (see Methods) the average Eddington ratio for FSRQs is reliable: $\langle L_{\text{disk}}/L_{\text{Edd}} \rangle = 0.1$ (Extended Data Figure 2). This implies that all FSRQ should have standard, geometrically thin, optically thick, accretion disks²⁶. Therefore the more powerful jets (the ones associated to FSRQs) *can* be produced by standard disks with presumably no central funnel, contrary to some expectations^{27,28}.

A related issue is the possible change of accretion regime at low accretion rate (in Eddington units), or, equivalently, when $L_{\text{disk}} \lesssim 10^{-2} L_{\text{Edd}}$. In this case the disk is expected to become radiatively inefficient, hotter and geometrically thick. How the jet responds to such changes is still an open issue. An extension of our study to lower luminosities could provide some hints. Another open issue is how the jet power depends on the black hole spin²⁹. Our source sample by construction consists of luminous γ -ray sources that presumably have the most powerful jets, and thus have the most rapidly spinning holes. It will be interesting to explore less luminous jetted sources, to get hints on the possible dependencies of the jet power on the black hole spin and the possible existence of a minimum spin value for the very existence of the jet. In turn, this should shed light on the long standing problem of the radio-loud/radio-quiet quasar dichotomy³⁰.

References

- [1] Blandford, R.D. & Znajek, R.L. Electromagnetic extraction of energy from Kerr black holes. *Mon. Not. R. Astr. Soc.* **179**, 433–456 (1977)
- [2] Rawlings, S. & Saunders, R., Evidence for a common central-engine mechanism in all extragalactic radio sources. *Nature* **439**, 138–140 (1991)
- [3] Celotti, A. & Fabian, A.C. The Kinetic Power and Luminosity of Parsecscale Radio Jets - an Argument for Heavy Jets. *Mon. Not. R. Astr. Soc.* **264**, 228–236 (1993)

- [4] Celotti, A., Padovani, P. & Ghisellini, G. Jets and accretion processes in Active Galactic Nuclei: further clues. *Mon. Not. R. Astr. Soc.* **286**, 415–424 (1997)
- [5] Maraschi, L. & Tavecchio, F. The Jet–Disk Connection and Blazar Unification. *Astrophys. J.* **593**, 667–675 (2003)
- [6] Punsly, B. & Tingay, S.J. PKS 1018–42: A Powerful, Kinetically Dominated Quasar. *Astrophys. J.* **640**, L21–L24
- [7] Celotti, A. & Ghisellini, G. The power of blazar jets. *Mon. Not. R. Astr. Soc.* **385**, 283–300 (2008)
- [8] Ghisellini, G., Tavecchio, F., Foschini, L., Ghirlanda, G., Maraschi, L. & Celotti, A. General physical properties of bright Fermi blazars. *Mon. Not. R. Astr. Soc.* **402**, 497–518 (2010)
- [9] Tchekhovskoy, A., Narayan, R. & McKinney, J.C. Efficient generation of jets from magnetically arrested accretion on a rapidly spinning black hole. *Mon. Not. R. Astr. Soc.* **418**, L79–L83 (2011)
- [10] Zamaninasab, M., Clausen–Brown, E., Savolainen, T. & Tchekhoskoy, A. Dynamically important magnetic fields near accreting supermassive black holes. *Nature* **512**, 126–128 (2014)
- [11] Thorne, K. Disk–Accretion onto a Black Hole. II. Evolution of the Hole. *Astrophys. J.* **191**, 507–519 (1974)
- [12] Shaw, M.S., Romani, R.W., Cotter, G., et al. Spectroscopy of broad–line Blazars from 1LAC. *Astrophys. J.* **748**, 49 (12pp) (2012)
- [13] Shaw, M.S., Romani, R.W., Cotter, G. et al. Spectroscopy of the Largest Ever γ –ray–selected BL Lac Sample. *Astrophys. J.* **764**, 135 (13pp) (2013)
- [14] Francis, J., Hewett, P.C., Foltz, C.B., Chaffee, F.H., Weymann, R.J. & Morris, S.L. A high signal–to–noise ratio composite quasar spectrum. *Astrophys. J.*, **373**, 465–470 (1991)
- [15] Vanden Berk, D.E., Richards, G.T. & Bauer, A. Composite Quasar Spectra from the Sloan Digital Sky Survey. *Astron. J.* **122**, 549–564 (2001)
- [16] Calderone, G., Ghisellini, G., Colpi, M. & Dotti, M. Black hole mass estimate for a sample of radio-loud narrow-line Seyfert 1 galaxies. *Mon. Not. R. Astr. Soc.* **431**, 210–239 (2013)
- [17] Ghisellini, G. & Tavecchio, F. Canonical high–power blazars. *Mon. Not. R. Astr. Soc.* **397**, 985–1002 (2009)
- [18] Ghisellini, G. & Tavecchio, F. Compton rockets and the minimum power of relativistic jets. *Mon. Not. R. Astr. Soc.* **409**, L79–L83 (2010)
- [19] Nolan P.L., Abdo A. A., Ackermann M., et al. Fermi Large Area Telescope Second Source Catalog. *Astrophys. J. Suppl.* **199**, 31 (46pp) (2012)

- [20] Ghirlanda, G., Ghisellini, G., Tavecchio, F., Foschini, L. & Bonnoli, G. The radio- γ -ray connection in *Fermi* blazars. *Mon. Not. R. Astr. Soc.* **413**, 852–862 (2011)
- [21] Nemmen, R.S., Georganopoulos, M., Guiriec, S., Meyer, E.T., Gehrels, N. & Samburina, R.M. A Universal Scaling for the Energetics of Relativistic Jets from Black Hole Systems. *Science* **338**, 1445–1448 (2012)
- [22] Tchekhovskoy, A., Metzger, B.D., Giannios, D. & Kelley, L.Z. Swift J1644+57 gone MAD: the case for dynamically important magnetic flux threading the black hole in a jetted tidal disruption event. *Mon. Not. R. Astr. Soc.* **437**, 2744–2760 (2014)
- [23] Peterson, B.M., Wandel, A. Evidence for Supermassive Black Holes in Active Galactic Nuclei from Emission-Line Reverberation. *Astrophys. J.* **540** L13–L16 (2000)
- [24] McLure, R.J. & Dunlop, J.S. The cosmological evolution of quasar black hole masses. *Mon. Not. R. Astr. Soc.* **352**, 1390–1404 (2004)
- [25] Vestergaard, M. & Peterson, B.M. Determining Central Black Hole Masses in Distant Active Galaxies and Quasars. II. Improved Optical and UV Scaling Relationships. *Astrophys. J.* **641**, 689–709 (2006)
- [26] Shakura, N.I. & Sunyaev, R.A. Black holes in binary systems. Observational appearance. *Astron. Astrophys.* **24**, 337–355 (1973)
- [27] Livio, M., Ogilvie, G.I. & Pringle, J.E. Extracting Energy from Black Holes: The Relative Importance of the Blandford-Znajek Mechanism. *Astrophys. J.* **512**, 100–104 (1999)
- [28] Meier, D.L. Grand Unification of AGN and the accretion and spin paradigms. *New Astron. Rev.* **46**, 247–255 (2002)
- [29] Tchekhovskoy, A., McKinney, J.C. & Narayan, R., General Relativistic Modeling of Magnetized Jets from Accreting Black Holes. *J. of Physics: Conference Series* **372**, Issue 1, id. 012040 (2012).
- [30] Sikora, M., Stawarz, L. & Lasota, J.–P. Radio Loudness of Active Galactic Nuclei: Observational Facts and Theoretical Implications. *Astrophys. J.* **658**, 815–828 (2007)

Acknowledgements FT and LM thank a PRIN–INAF 2011 grant for partial funding.

Author Contributions GG wrote the manuscript and fitted all blazars presented. FT, LM, AC and TS contributed to the discussion for the implications of our results.

Author information Reprints and permissions information is available at www.nature.com/reprints. The authors declare no competing financial interests. Correspondence and requests for materials should be addressed to G.G. (gabriele.ghisellini@brera.inaf.it).

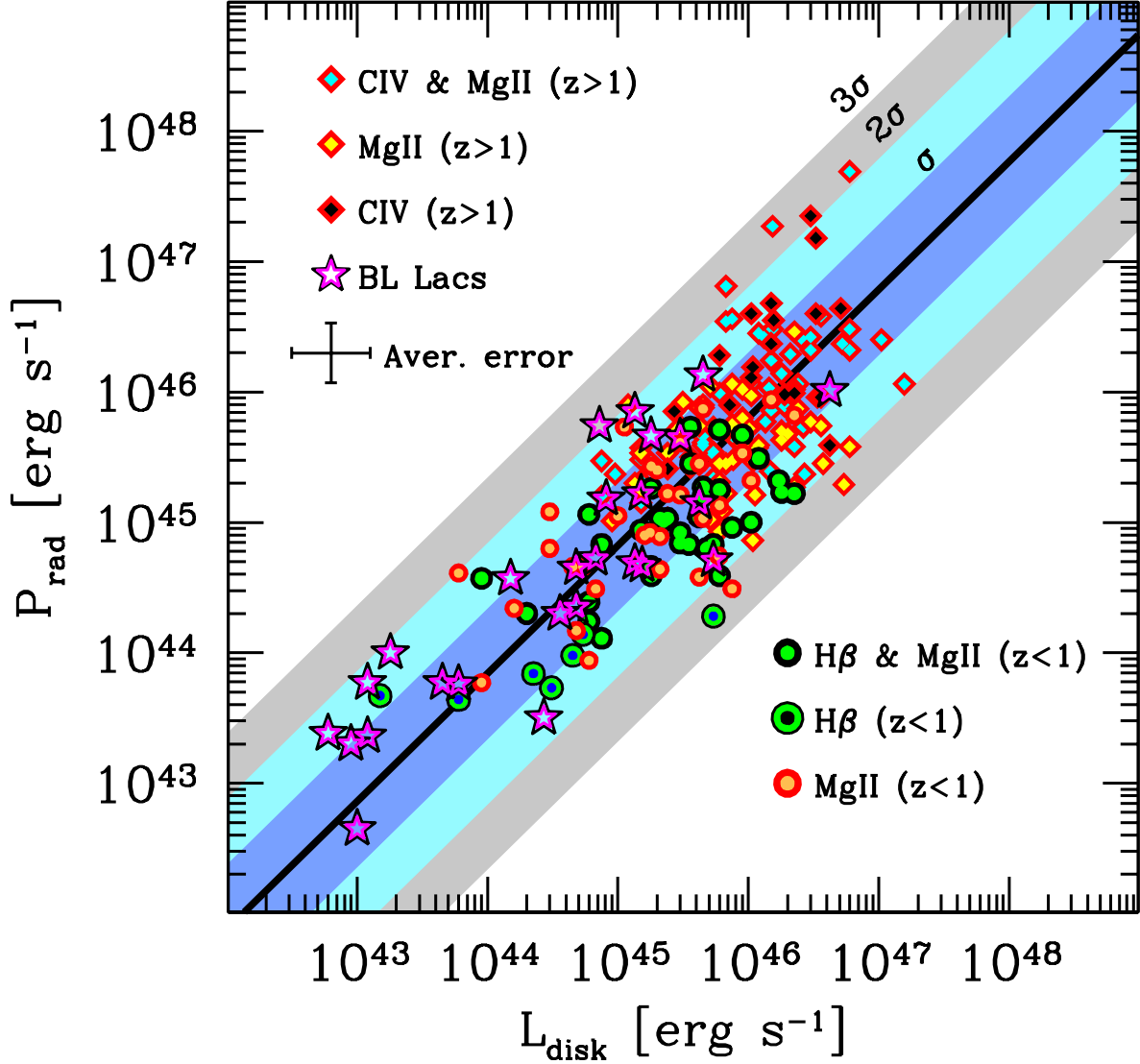


Figure 1: **Radiative jet power vs disk luminosity.** The radiative jet power versus the disk luminosity, calculated as ten times the luminosity of the Broad Line Region. Different symbols correspond to the different emission lines used to estimate the disk luminosity, as labelled. All objects have been detected by *Fermi*/LAT and have been spectroscopically observed in the optical^{12,13}. Shaded colored areas correspond to 1, 2 and 3 σ (vertical) dispersion. $\sigma = 0.5$ dex. The black line is the best least square fit ($\log P_{\text{rad}} = 0.98 \log L_{\text{disk}} + 0.639$). The average error bar corresponds to an uncertainty of a factor 2 in L_{disk} ¹⁶ and 1.7 in P_{rad} (corresponding to the uncertainty in Γ^2).

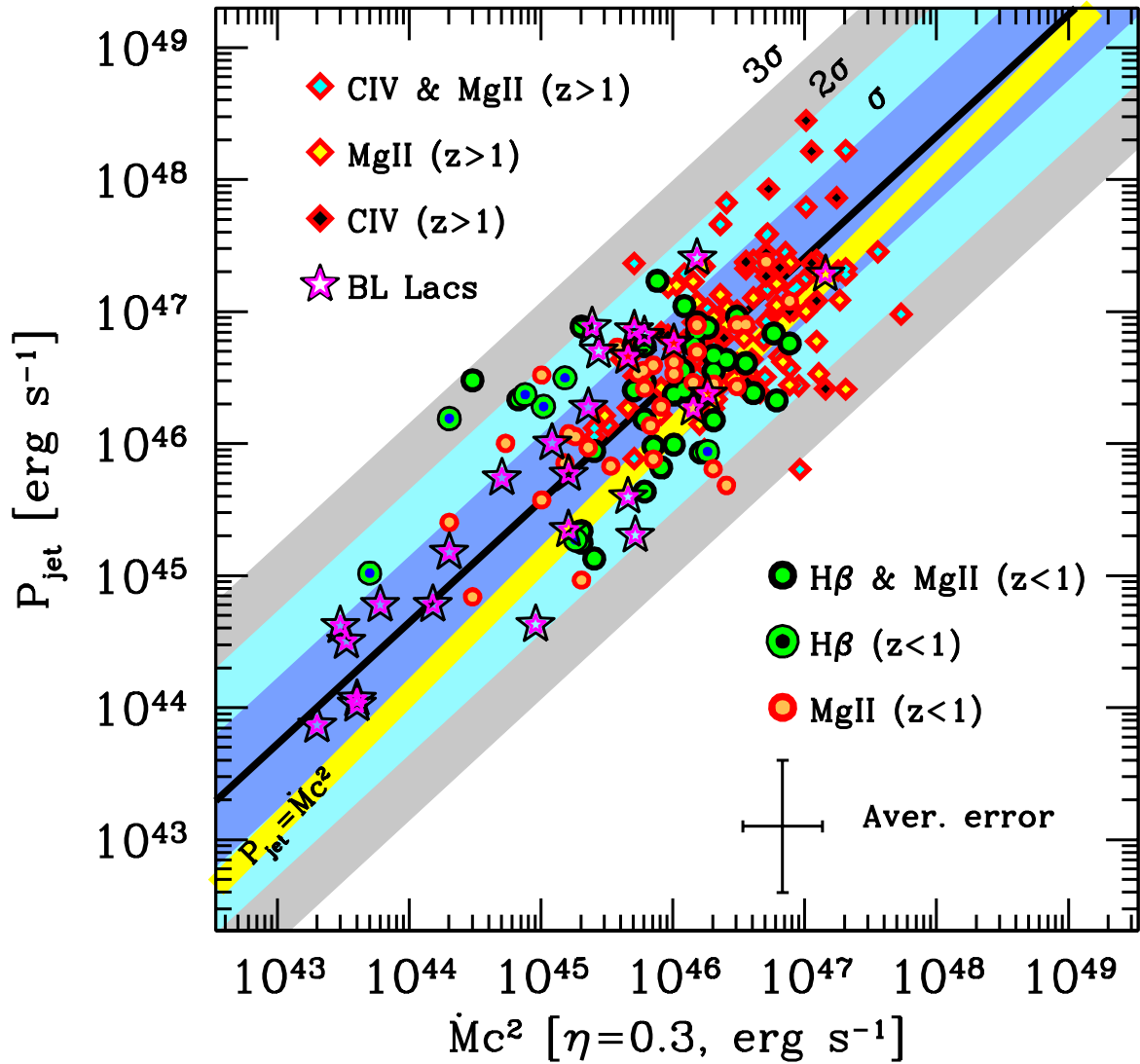


Figure 2: **Jet power vs accretion power.** The total jet power estimated through a simple one-zone leptonic model¹⁷, assuming one cold proton per emitting electron, vs $\dot{M}c^2$ calculated assuming an efficiency $\eta = 0.3$, appropriate for a maximally rotating Kerr Black hole. Different symbols correspond to the different emission lines used to estimate the disk luminosity, as in Fig. 1. Shaded colored areas correspond to 1, 2 and 3 σ (vertical) dispersion. $\sigma = 0.5$ dex. The black line is the best least square fit [$\log P_{\text{jet}} = 0.92 \log(\dot{M}c^2) + 4.09$]. The yellow stripe is the equality line. The average error bar is indicated ($\dot{M}c^2$ has the same average uncertainty of L_{disk} ; the average uncertainty P_{jet} is a factor 3).

METHODS

The sample. Our sample is composed by 229 blazars detected by *Fermi*/LAT^{31,33} for which broad emission lines have been measured^{12,13,32}. This sample does not include several bright and famous blazars with historical spectroscopic classifications in the literature. Of these, we have studied the 217 objects with enough multiwavelength information necessary to apply our model. Within the sample, we have 26 BL Lac objects with measured broad emission lines¹³. Therefore our “BL Lac” objects, even if fulfilling the classical definition of BL Lacs (emission lines of equivalent width smaller than 5 Å), are not lineless, and can be considered as the low disk luminosity tail of the blazar sample.

This is the largest ever sample of γ -ray detected sources with measured broad emission lines. From these lines we can estimate the luminosity L_{BLR} of the entire broad line region (BLR), using standard templates^{14,15}. Then we calculate the disk luminosity by assuming that $L_{\text{disk}} = 10L_{\text{BLR}}$, with an average uncertainty¹⁶ of a factor 2. Since the lines are isotropically emitted, the estimate of L_{disk} does not depend on the viewing angle. Moreover, L_{disk} estimated from L_{BLR} does not depend on any contamination of non-thermal components. In a few cases (20 out of 217, Extended Data Table 1) the resulting L_{disk} contrasts by a factor between 2 and 5 with the value of L_{disk} given by fitting a standard accretion disk, that better fits the optical-UV data. In these cases we have chosen the value of L_{disk} given by the disk fitting. From the knowledge of the SED, often dominated by the γ -ray luminosity, we can estimate the bolometric jet luminosity in a reliable way. The knowledge of the disk luminosity and the black hole mass greatly helps to fix two important parameters for the theoretical modelling, helping to find a unique solution for the considered emitting region of the jet. Although the mass estimate can be affected by a rather large statistical error, there should be no relevant systematic error, since a completely independent method^{34,35} led to consistent values.

The bolometric jet luminosity. The spectral energy distribution (SED) of blazars is characterized by two broad humps [in the $\nu L(\nu)$ vs ν representation, where ν is the emission frequency], peaking in the mm-UV and in the MeV-GeV bands. The high energy bump is often the dominant component, except for low power (and lineless) BL Lacs^{36,37}, in which the synchrotron luminosity is more important. This is the reason to select *Fermi*/LAT detected blazars: for these objects we can assess the jet bolometric luminosity with high confidence. However, the amplitude of variability, especially in the γ -ray band, can be larger than 2 orders of magnitude, and even larger if one includes exceptionally high states, as the ones experienced by 3C 454.3³⁸. Taking the mean luminosity over a period of two years averages out short term variability, but not the secular (>10 yr timescale) one. The γ -ray luminosity measured in *detected* sources could not represent the average status of the source, but only its high state. On the other hand, the γ -ray luminosity correlates with the radio one²⁰, and a Gaussian distribution of long term γ -ray variability with $\sigma = 0.5$ dex (i.e. a factor 3), coupled with the *Fermi*/LAT sensitivity, can fully explain what is observed, including the fact that several strong radio sources are yet undetected in the γ -rays. As a result, the observed correlations in Figg. 1 and 2 could represent jet-active states, rather than the average state, that could correspond to a jet power P_{jet} up to a factor ~ 3 smaller. However, the radio- γ correlation gives us confidence that P_{jet} would still be correlated with L_{disk} and \dot{M} . The fact that the process of forming and launching

relativistic jets is more powerful than accretion only in jet–active states does not affect the conclusion that this process is indeed more powerful than accretion, even if it does not always works at its maximum pace.

The model used. We summarize here the main features of the used model³⁹. It assumes that the jet region emitting most of the non–thermal luminosity is at a distance R_{diss} from the black hole. For this reason this class of models is called “one–zone”, and they are justified because often (although not always) we see coordinated variability at different frequency bands. The jet is assumed conical with semi–aperture angle ψ . We assume $\psi = 0.1$ ⁴⁰, but the exact value is not critical for our results. The emitting region is assumed spherical, with radius $R = \psi R_{\text{diss}}$, embedded in a homogeneous but tangled magnetic field B . The emitting particles are leptons (requiring less power than the less common alternative of emitting hadrons⁴¹). The main feature of the model is that it accounts for the radiation fields produced by the emission disk, the broad line region, the dusty torus surrounding the disk and re–emitting part of the intercepted radiation in the infrared. The distance of the BLR is assumed to be a function of the disk luminosity, as indicated by recent observations (through the so–called reverberation mapping technique⁴²): $R_{\text{BLR}} = 10^{17} L_{\text{d},45}^{1/2}$ cm. We assume that also the typical size of the molecular torus scales similarly: $R_{\text{torus}} = 2 \times 10^{18} L_{\text{d},45}^{1/2}$ cm (in agreement with very recent reverberation results⁴³). Here $L_{\text{d},45}$ is the disk luminosity in units of 10^{45} erg s^{−1}. As a consequence, inside the BLR, the radiative energy density corresponding to broad lines is constant: $U_{\text{BLR}} \sim 0.1 L_{\text{disk}} / [4\pi R_{\text{BLR}}^2 c] = 1/(12\pi)$ erg cm^{−3}. A similarly expression holds for the energy density of the IR photons of the torus.

The particle distribution responsible for the produced radiation is derived through a continuity equation assuming continuous injection of relativistic leptons at R_{diss} , their radiative cooling, the possible production of electron–positron pairs through photon–photon collisions and their corresponding radiation. The energy distribution of the injected particles is a broken power–law, flat at low energies and steepening above some break energy γ_{b} . Since the considered emitting region is always compact, its self–absorption frequency is always large, and the model cannot account for the radio flux at observed frequencies smaller than a few hundreds GHz. These are produced by the superposition of several, larger, components. The emission produced by the accretion disk is assumed to be a multicolor blackbody, with a temperature distribution dictated by the balance of heat production and radiative dissipation²⁶. The corresponding values of L_{disk} found through disk fitting are listed in the Extended Data Table 1.

Although the model returns several physical parameters, we concentrate on the ones of interest here: the bulk Lorentz factor Γ and Doppler factor δ , the location of the emitting region and the jet power.

The bulk Lorentz factor Γ and Doppler factor δ . The bulk Lorentz factor, coupled with the viewing angle θ_{v} , determines the Doppler factor $\delta \equiv 1/[\Gamma(1 - \beta \cos \theta_{\text{v}})]$. For blazars, we have $\sin \theta_{\text{v}} \sim 1/\Gamma$ and thus $\delta \sim \Gamma$. There are several observables affected by Γ :

i) The observed $\nu F(\nu)$ flux is amplified by a factor δ^4 with respect to the comoving value for the synchrotron (Syn) and the self Compton (SSC) emission, and more for the flux produced through scattering with photons produced external to the jet⁴⁴ (this is because, in the comoving frame, the external seed photons are not isotropic, but coming

from the forward direction).

ii) As long as the emitting region is inside the BLR, the corresponding energy density is amplified by a factor $\sim \Gamma^2$ (independently of θ_v). Similarly for the IR emission coming from the torus. If $R_{\text{diss}} < R_{\text{BLR}}$, the external Compton (EC) process most likely dominates over the SSC process, and the Compton to synchrotron luminosity ratio (equal to the radiative to magnetic energy density ratio in the comoving frame: U'_{BLR}/U'_B) becomes proportional to $(\Gamma/B)^2$. The same occurs for the IR radiation reprocessed by the torus as long as $R_{\text{diss}} < R_{\text{torus}}$.

iii) The Doppler boosting regulates the importance of the SSC component. In brief: the larger the δ factor, the smaller the synchrotron radiation energy density in the comoving frame, and therefore the smaller the SSC component.

iv) The Doppler factor blueshifts the observed peak frequencies.

In conclusion, there are several observables that depend on combinations of parameters that include the Γ and the δ factors. Finding the best representation of the data thus implies to find a preferred value for these parameters.

By modelling the 217 blazars of our sample we find a rather narrow distribution of the bulk Lorentz factors, peaking at $\Gamma \sim 13$ (Extended Data Figure 2). A Gaussian fit returns a dispersion of $\sigma = 1.4$. The (few) studied BL Lac objects do not show any difference from FSRQs.

The jet power. The power carried by the jet is in different forms, calculated as:

$$P_i = 2 \pi R^2 \Gamma^2 c U'_i \quad (2)$$

where the factor 2 accounts for having two jets and U'_i is the comoving energy density of protons (i=p), relativistic electrons (i=e), magnetic field (i=B) and of the produced radiation (i=rad). The radiative power P_{rad} can also be found through¹⁸:

$$\begin{aligned} P_{\text{rad}} &= 2 \times \frac{4}{3} L_{\text{bol,jet}}^{\text{obs}} \frac{\Gamma^2}{\delta^4}, & \text{EC} \\ P_{\text{rad}} &= 2 \times \frac{16}{5} L_{\text{bol,jet}}^{\text{obs}} \frac{\Gamma^4}{\delta^6}, & \text{Syn and SSC} \end{aligned} \quad (3)$$

This is the way P_{rad} has been calculated: Eq. 1 is the approximation for $\delta \sim \Gamma$, and where f corresponds to the numerical factor (4/3) or (16/5).

The main logic is: by applying a radiative model, we derive how much magnetic field and how many emitting leptons are required to account for the observed luminosity, and also the size and the bulk Lorentz factor of the emitting region. We then assume that *all* leptons present in the jet participate to the emission, and that for each lepton there is a proton. We assume them cold, even if shock acceleration and/or magnetic reconnection would give at least equal energy to the leptons and to the protons. This simplification is reasonable as long as the average electron energy remains smaller than the proton rest-mass.

The power P_{rad} is a *lower limit* to the power because if the total jet power were P_{rad} , then it would convert all its bulk kinetic energy to produce the radiation we see, and it would stop, well before we see it still moving, i.e. with Very Large Baseline Interferometry (VLBI) observations, that samples a region pc away from the black hole. The distributions of the different forms of the jet power are shown in the Extended Data Fig. 3, where they

are compared with the distribution of L_{disk} . To account for P_{rad} , the Poynting flux and P_e are not sufficient. We do need another form of power. The simple solution is to assume that the jet carries enough protons to have $P_p > P_{\text{rad}}$. This is strengthened by the fact that if the jet were made up of pairs only, it would suffer a strong deceleration due to the Compton rocket effect when crossing the broad line region, and it would stop. In fact, in the comoving frame of the jet, the external photons are seen coming from the forward direction. Even if the leptons are distributed isotropically, head-on scatterings along the forward direction of the jet axis would be more frequent and energetic than tail-on scatterings. The produced radiation, in the jet comoving frame, has a forward momentum, compensated by a recoil of the jet emitting region. With no protons, the jet strongly decelerates. Not to have a strong (i.e. halving Γ) deceleration¹⁸, the number of pairs should not exceed ~ 10 – 20 per proton, in agreement with estimates made with independent methods^{7, 18, 45}.

Jet power and location of the emitting region. The location of the emitting region could impact on the required jet power. The emitting region is estimated to be at distances $R_{\text{diss}} < R_{\text{BLR}}$ (85% of the sources) or at $R_{\text{BLR}} < R_{\text{diss}} < R_{\text{torus}}$ (15% of the sources). This is dictated by the SED properties (i.e. if the Compton peak is at \sim MeV energies a smaller frequency seed external field is preferred). Locating the source much further out, where there are no important sources of external photons, would increase the jet power requirements, as shown below. We have the following two possibilities:

1) the SED could result from Synchrotron+SSC. In this case the parameters can be found univocally⁴⁶. The synchrotron ν_S and Compton ν_C peak frequencies ratio gives γ_{peak}^2 . The Compton dominance (Compton to synchrotron luminosity ratio L_C/L_S) and the definition of $\nu_S = 3.6 \times 10^6 \gamma_{\text{peak}}^2 \delta / (1+z)$ give:

$$B\delta^2 = \frac{L_{\text{syn}}}{R} \left[\frac{2}{cL_C} \right]^{1/2}; \quad B\delta = \frac{\nu_S^2}{3.6 \times 10^6 \nu_C (1+z)} \quad (4)$$

Solving for B and δ , (setting $R = ct_{\text{var}}\delta/(1+z)$) and inserting typical values of the observables (i.e. $t_{\text{var}} \sim 1$ day, $\nu_S \sim 10^{13}$ Hz, $\nu_C \sim 10^{22}$ Hz, $L_S \sim 10^{46}$ erg s⁻¹ and $L_C \sim 10^{47}$ erg s⁻¹) one finds small B ($\lesssim 10^{-4}$ Gauss) and large δ ($\gtrsim 100$). A large δ in turn requires very small viewing angles ($< 1^\circ$, causing problems with determining the number of the sources belonging to the parent population) and large Γ . As a consequence, the energy densities inside the source are very small, making the cooling time very long. Invoking the second order SSC does not help, since all comoving radiation energy densities are small, because δ is large. The pure SSC process, applied to the sources in our sample, is thus very inefficient. This implies that more emitting electrons are needed to produce the observed flux, even accounting for the larger beaming. P_{rad} is small (because it is $\propto \Gamma^{-2}$), but P_e is increased. The source is away from equipartition, and its total minimum power is greater than it would be if the source were in a dense external photon environment⁴⁷. We have directly experimented this by applying the pure SSC model to some sources. In the case of 0325+2224, at $z=2.066$, we derive: $\text{Log } P_{\text{rad}}=44.9$, $\text{Log } P_p=48.6$, $\text{Log } P_e=47.3$ and $\text{Log } P_B=42.4$, to be compared with the values in Extended Data Table 1. Far from sources of external photons (i.e. pure SSC) the required total jet power *increases*. Having two emitting regions (one for the synchrotron, another for the inverse Compton components) does not help, because the component emitting the γ -rays must produce less synchrotron

radiation than we see, requiring an even smaller magnetic field: the radiative cooling is even less, and the entire process is even less efficient. Since the probability that a single emitting region is aligned within 1° to the observer (as required by the large delta) is very small, there must be several of these small regions pointing in different directions. The power that we calculate on the basis of observations refers to only one of these regions. The total jet power is bound to be much more.

2) The SED is made by a Spine/Layer structure, i.e. a slow layer surrounding a fast spine. The layer emits, and its photons are scattered by the spine, enhancing its Compton flux with respect to the pure SSC case. The radiative cooling is then more efficient. This model is very similar to the one we used, with one difference: using the external photons made by the BLR and the torus is “for free”, while using the photons made by the layer implies that the jet puts some energy and power also in the layer, besides in the spine. This model therefore inevitably implies a more powerful jet.

Low energy electrons and jet power. The energy distribution of injected electrons has a flat slope ($\propto \gamma^{-s_1}$) at low energies, with $-1 < s_1 < 1$. We then calculate the particle distribution $N(\gamma)$ at the time R_{blob}/c , and the cooling energy γ_{cool} at this time. Electrons of energy $\gamma < \gamma_{\text{cool}}$ retain the injected slope. Due to the flat s_1 , the number of electrons between $\gamma \sim 1$ and γ_{cool} is small compared to the number of electrons above γ_{cool} . In the EC scenario, low energy electrons are responsible for the X-ray spectrum, so the value of γ_{cool} is constrained by the data. The total number of emitting electron is well constrained.

Electron positron pairs and jet power. If electron positron pairs are present, the number of protons is reduced, with a corresponding reduction of the jet power, up to a factor 10 (not to suffer a too strong Compton rocket effect). On the other hand, producing the required number of pairs is problematic. In fact they *cannot* be produced at R_{diss} . They would be relativistic from the start and emit X-rays, filling the “valley” in the X-ray part of the SED⁴⁸. They *cannot* be produced by the accretion disk, which is too cold. The only possible source is the initial, accelerating part of the jet, whose observed radiation is overwhelmed by the much more beamed flux produced at R_{diss} . This possibility requires a self absorbed synchrotron flux and quasi-thermal Comptonization making the spectrum to peak exactly at 1 MeV⁴⁹. A peak at higher energies implies pairs born relativistic and fewer in number; a peak below the pair production threshold $m_e c^2$ implies too few produced pairs. We find this scenario rather ad hoc and very unlikely to occur in all sources.

Consider also that:

i) If P_{jet} is lowered by a factor 10 then almost half of the sources in our sample would have $P_{\text{jet}} < P_{\text{rad}}$ (Fig. 1): this implies that the jet stops at R_{diss} (and no radio halo, no superluminal motion would be possible); ii) It is found that $P_{\text{jet}} \sim 10P_{\text{rad}}$ for blazars and for Gamma Ray Burst, using arguments completely different from ours²¹.

References

- [31] Abdo, A.A., Ackermann, M., Ajello, M. et al. The First Catalog of Active Galactic Nuclei Detected by the Fermi Large Area Telescope. *Astrophys. J.* **715**, 429–457 (2010)

- [32] Shen, Y., Richards, G.T., Strauss, M.A. et al. A Catalog of Quasar Properties from Sloan Digital Sky Survey Data Release 7. *Astrophys. J. Supp.* **194**, 45 (21 pp) (2011)
- [33] Ackermann, M., Ajello, M., Allafort, A. et al. The Second Catalog of Active Galactic Nuclei Detected by the Fermi Large Area Telescope. *Astrophys. J.* **743**, 171 (37 pp) (2011)
- [34] Ghisellini, G. Extragalactic relativistic jets. 25th Texas Symp.. AIP Conf. Proceed. **1381**, 180–198 (2011) (arXiv:1104.0006)
- [35] Sbarrato, T., Ghisellini, G., Nardini, M., Tagliaferri, G., Greiner, J., Rau, A. & Schady, P. Blazar candidates beyond redshift 4 observed with GROND *Mon. Not. R. Astr. Soc.* **433**, 2182–2193 (2013)
- [36] Fossati, G., Maraschi, L., Celotti, A., Comastri, A. & Ghisellini, G. A unifying view of the spectral energy distributions of blazars. *Mon. Not. R. Astr. Soc.* **299**, 433–448 (1998)
- [37] Donato, D., Ghisellini, G., Tagliaferri, G. & Fossati, G. Hard X-ray properties of blazars. *Astron. Astrophys.* **375**, 739–751 (2001)
- [38] Bonnoli, G., Ghisellini, G., Foschini, L., Tavecchio, F. & Ghirlanda, G. The γ -ray brightest days of the blazar 3C 454.3. *Mon. Not. R. Astr. Soc.* **410**, 368–380 (2011)
- [39] Ghisellini, G. & Tavecchio, F. Canonical high-power blazars. *Mon. Not. R. Astr. Soc.* **397**, 985–1002 (2009)
- [40] Nalewajko, K., Begelman, M.C. & Sikora, M. Constraining the Location of Gamma-Ray Flares in Luminous Blazars. *Astrophys. J.* **789**, 161, 20pp (2014)
- [41] Böttcher, M., Reimer, A., Sweeney, K. & Prakash, A. Leptonic and Hadronic Modeling of Fermi-detected Blazars. *Astrophys. J.* **768**, 54 14 pp (2013)
- [42] Bentz, M.C., Peterson, B.M., Pogge, R.W., Vestergaard, M. & Onken, C.A. The Radius–Luminosity Relationship for Active Galactic Nuclei: The Effect of Host–Galaxy Starlight on Luminosity Measurements. *Astroph. J.* **644**, 133–142 (2006)
- [43] Koshida, S., Minezaki, T., Yoshii, Y., et al. Reverberation measurements of the inner radius of the dust torus in 17 Seyfert galaxies. *Astrophys. J.* **788**, 159, 21pp (2014)
- [44] Dermer, C. On the Beaming Statistics of Gamma-Ray Sources. *Astrophys. J.* **446**, L63–L66 (1995)
- [45] Sikora, M. & Madejski, G. On Pair Content and Variability of Subparsec Jets in Quasars. *Astrophys. J.* **534**, 109–113 (2000)
- [46] Tavecchio, F., Maraschi, L. & Ghisellini, G. Constraints on the Physical Parameters of TeV Blazars. *Astrophys. J.* **509**, 608–619 (1998)
- [47] Ghisellini, G. & Celotti, A. Relativistic large-scale jets and minimum power requirements. *Mon. Not. R. Astr. Soc.* **327**, 739–743 (2001)
- [48] Ghisellini, G. & Madau, P. On the origin of the gamma-ray emission in blazars. *Mon. Not. R. Astr. Soc.* **280**, 67–76 (1996)

- [49] Ghisellini G. Electron-positron pairs in blazar jets and γ -ray loud radio galaxies. *Mon. Not. R. Astr. Soc.* **424**, L26–L30 (2012)

EXTENDED DATA

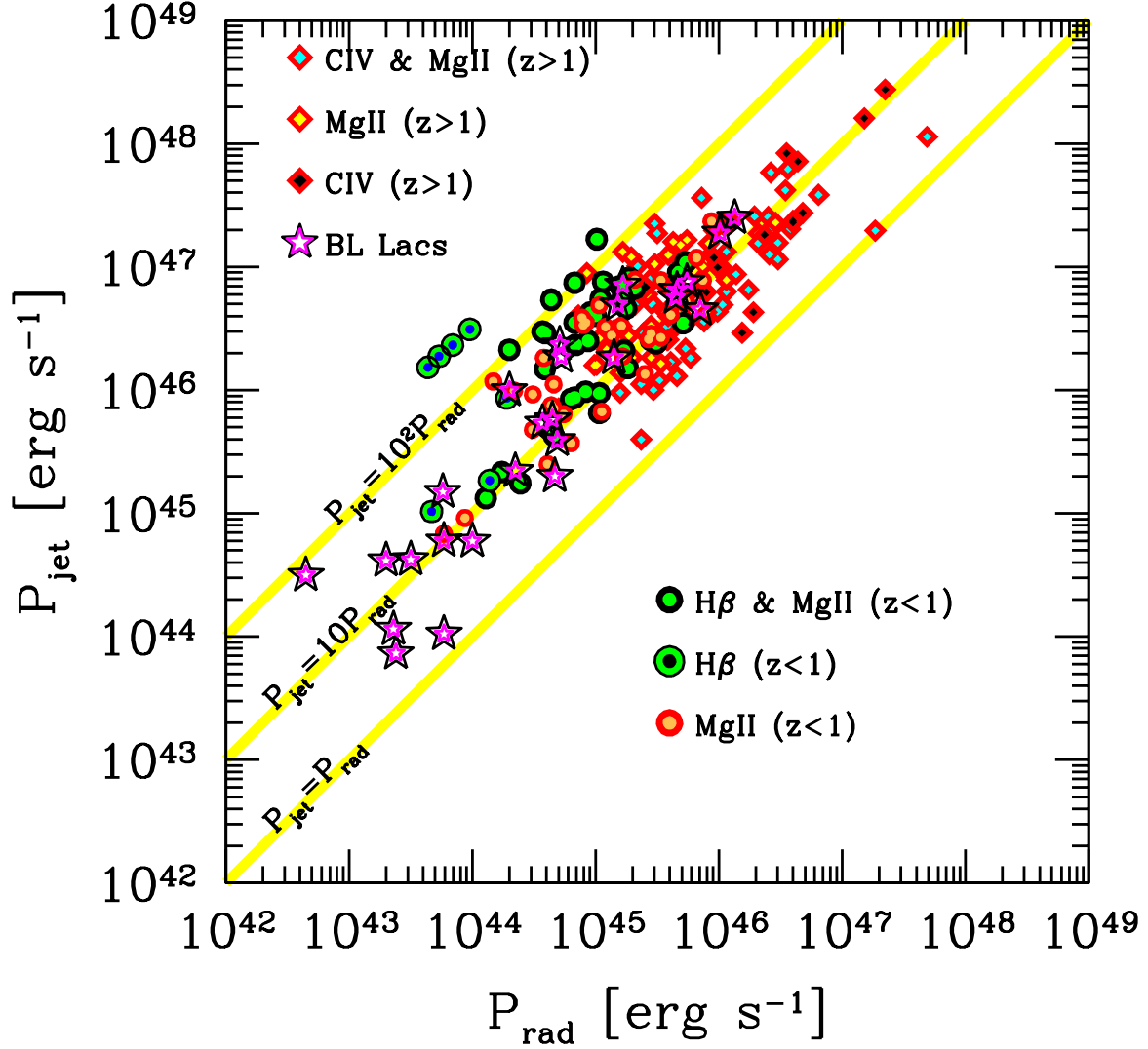


Figure 1: **Extended Data Figure 1: Jet power vs radiative jet power.** We compare the total jet power and the radiative one for the blazars in our sample. The yellow lines, as labelled, correspond to equality and to P_{jet} equal to 10-fold and 100-fold P_{rad} . Same symbols as in Fig. 1. The average error bar is indicated.

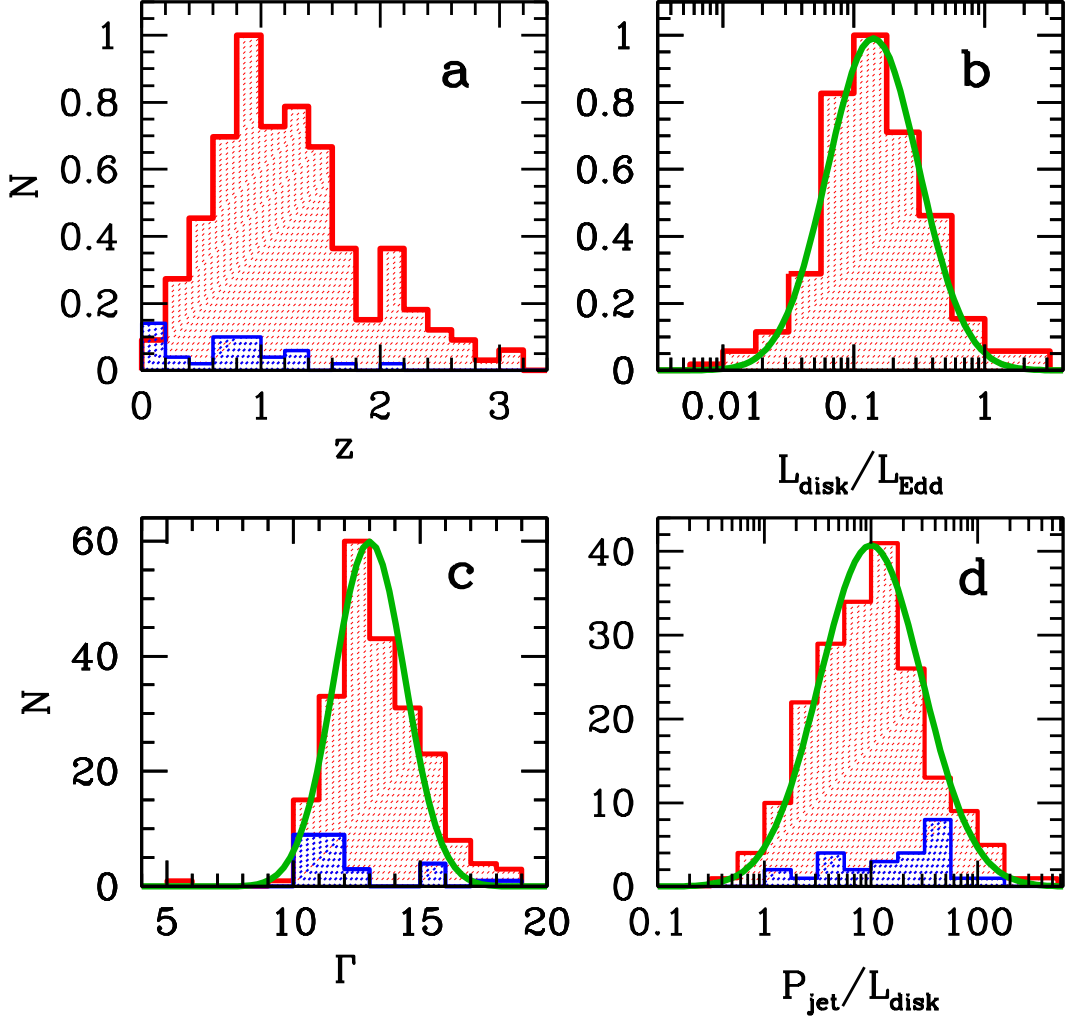


Figure 2: **Extended Data Figure 2: Distribution of relevant quantities.** **a:** Normalized redshift distribution for FSRQ (red hatching) and BL Lacs (blue hatching) in our sample. **b:** Normalized distribution of the ratio $\log L_{\text{disk}}/L_{\text{Edd}}$ for the FSRQs in our sample. The black hole mass is the virial mass, calculated on the basis of the width of the broad lines¹², compared to a log-normal distribution having a width $\sigma = 0.35$ dex. **c:** Distribution of the bulk Lorentz factor. The darker hatched histogram corresponds to BL Lacs. The plotted gaussian distribution has a width $\sigma = 1.4$. **d:** Distribution of the ratio $\log P_{\text{jet}}/L_{\text{disk}}$ for our sources, including BL Lacs (darker hatched histogram). The shown log-normal distribution has a width $\sigma = 0.48$ dex.

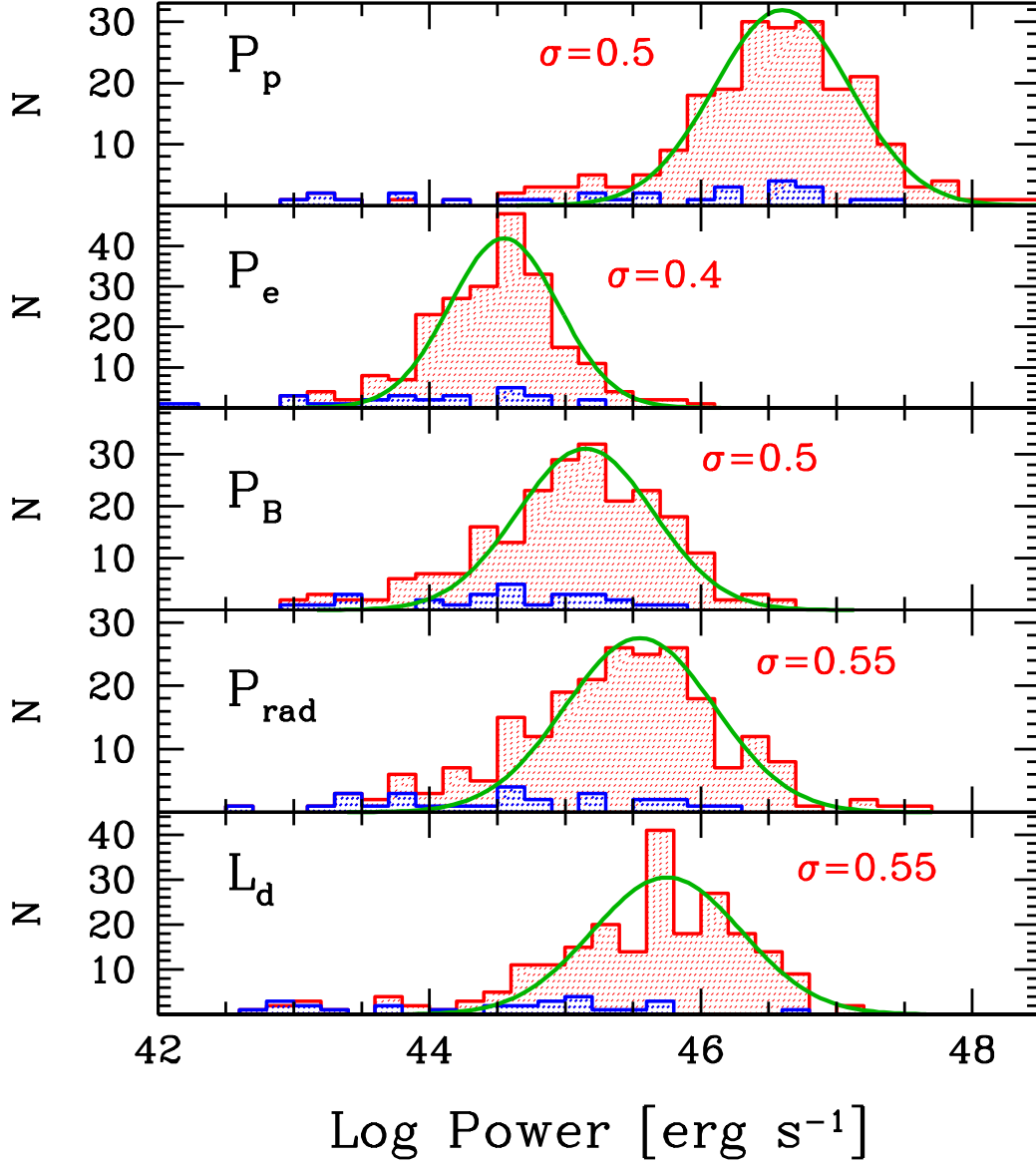


Figure 3: **Extended Data Figure 3: Distribution of jet powers.** Jet power distribution for FSRQ and BL Lacs (darker hatched histogram) in our sample, compared with the disk luminosity distribution as labelled: P_p is the kinetic power of the (cold) protons, assuming on proton per emitting electron; P_e is the power in relativistic emitting electrons; P_B is the jet Poynting flux; P_{rad} is the power that the jet has spent to produce the observed radiation; L_{disk} is the luminosity of the accretion disk. All distributions are fitted with a log-normal distribution. The corresponding value of σ (in dex) is reported. The average values of the distributions are: $\langle \log L_{\text{disk}} \rangle = 45.5$, $\langle \log P_{\text{rad}} \rangle = 45.3$, $\langle \log P_B \rangle = 45.0$, $\langle \log P_e \rangle = 44.4$, $\langle \log P_p \rangle = 46.4$ (units are erg s^{-1}).

Name	z	P_{rad}	P_e	P_B	P_p	Γ	θ_v	$L_{\text{disk,fit}}$	$L_{\text{disk,l}}$	$M_{\text{H}\beta}$	M_{MgII}	M_{CIV}
[1]	[2]	[3]	[4]	[5]	[6]	[7]	[8]	[9]	[10]	[11]	[12]	[13]
0004-4736	0.880	44.64	43.98	44.93	45.79	14.0	2.0	45.32	45.11	—	7.85	—
0011+0057	1.493	45.50	44.80	44.87	47.27	13.0	3.0	45.56	45.60	—	7.80	7.09
0015+1700	1.709	45.58	44.16	45.66	46.45	12.0	3.0	46.35	46.26	—	9.36	9.15
0017-0512	0.226	43.98	44.04	43.87	46.49	12.0	3.0	44.65	45.30	7.55	—	—
0023+4456	2.023	45.85	44.88	45.16	46.75	15.0	3.0	45.43	45.28	—	—	7.78
0024+0349	0.545	43.94	43.17	44.38	44.76	13.0	3.0	44.78	44.79	—	7.76	—
0042+2320	1.426	45.74	44.96	45.01	47.20	13.0	3.0	45.62	45.62	—	9.01	—
0043+3426	0.966	45.05	44.05	44.31	45.72	14.0	3.0	45.00	45.02	—	7.01	—
0044-8422	1.032	45.48	44.72	45.27	47.00	14.0	3.0	45.88	45.88	—	7.68	—
0048+2235	1.161	45.46	44.53	44.56	46.70	13.0	3.0	45.26	45.26	—	7.43	7.25
0050-0452	0.922	44.89	44.39	44.74	46.57	11.0	3.0	45.32	45.35	—	7.20	—
0058+3311	1.369	45.15	44.43	44.48	46.48	13.0	3.0	45.18	45.21	—	7.01	7.97
0102+4214	0.874	45.25	44.45	45.09	46.63	12.0	3.0	45.78	45.83	7.92	7.49	—
0102+5824	0.644	45.03	44.40	45.26	46.66	11.0	3.0	45.65	45.66	—	7.57	—
0104-2416	1.747	45.63	44.59	45.39	46.51	11.0	3.0	45.91	45.94	—	7.85	7.97
0157-4614	2.287	45.99	44.71	45.08	46.62	14.0	3.0	45.78	45.73	—	7.98	7.52
0203+3041	0.955	45.08	44.66	43.79	46.49	13.0	3.0	44.48	44.40	—	7.02	—
0217-0820	0.607	44.34	43.98	43.78	45.98	13.0	3.0	44.20	44.06	—	6.53	—
0226+0937	2.605	45.59	44.03	45.93	46.12	12.0	3.0	46.62	46.53	—	—	9.65
0237+2848	1.206	45.70	44.69	45.68	47.00	13.0	3.0	46.26	46.38	—	9.22	—
0245+2405	2.243	46.29	44.95	45.63	47.40	14.0	3.0	46.32	46.33	—	9.02	9.18
0246-4651	1.385	46.06	44.94	46.08	47.08	12.0	3.0	46.38	46.42	—	7.48	7.32
0252-2219	1.419	45.92	44.90	45.20	47.16	12.0	3.0	45.50	45.72	—	9.40	—
0253+5102	1.732	46.06	44.66	45.33	46.78	14.0	3.0	46.02	45.99	—	9.11	7.37
0257-1212	1.391	45.27	44.15	45.66	46.32	11.0	3.0	46.35	46.13	—	9.22	—
0303-6211	1.348	45.77	44.57	46.26	46.87	11.0	3.0	46.48	46.64	—	9.76	—
0309-6058	1.479	46.06	44.83	45.48	46.80	13.0	3.0	45.88	45.88	—	7.87	—
0315-1031	1.565	45.44	44.62	44.93	46.89	13.0	3.0	45.62	45.67	—	7.17	7.33
0325+2224	2.066	46.32	45.06	46.09	47.24	12.0	3.0	46.78	46.79	—	9.50	9.16
0325-5629	0.862	44.58	43.92	44.94	46.23	10.0	3.0	45.62	45.60	—	7.68	—
0407+0742	1.133	45.31	44.56	45.38	46.83	12.0	3.0	45.78	45.51	—	7.65	—
0413-5332	1.024	45.25	44.66	44.49	46.66	12.0	3.0	45.18	45.14	—	7.83	—
0422-0643	0.242	43.73	43.83	44.10	46.27	12.0	3.0	44.49	44.42	7.47	—	—
0430-2507	0.516	43.77	43.15	43.56	44.76	11.0	3.0	43.95	43.81	—	6.51	—
0433+3237	2.011	45.35	44.22	45.37	46.88	13.0	3.0	46.56	46.58	—	9.17	9.20
0438-1251	1.285	45.09	44.35	45.11	46.27	11.0	3.0	45.80	45.78	—	7.66	—
0442-0017	0.845	45.71	44.59	45.09	46.45	13.0	3.0	45.78	45.81	7.74	7.46	—
0448+1127	1.370	45.87	44.55	45.39	46.96	16.0	3.0	46.38	46.71	—	9.44	—
0449+1121	2.153	45.90	45.16	45.24	46.71	13.0	2.5	45.86	45.92	—	—	7.89
0456-3136	0.865	44.84	44.20	44.79	46.34	13.0	3.0	45.48	45.26	7.78	7.61	—

Table 1: **Extended Data Table 1: Relevant parameters of the blazars studied in this paper.**

Col. 1 and Col. 2 : AR and Dec (J2000); Col. 2: redshift; Col. 3 – Col. 6: Logarithm of P_{rad} , P_e , P_B , P_p (powers in units of erg s^{-1}); Col. 7: bulk Lorentz factor; Col. 8: viewing angle in degrees; Col. 9: Logarithm of the disk luminosity (in units of erg s^{-1}) as resulting from disk fitting; Col. 10: Logarithm of the disk luminosity (in units of erg s^{-1}) as measured from the broad emission lines; Col. 11 – Col. 13: logarithm of the black hole mass (in units of the solar mass) estimated through the virial method¹² using the H β (Col. 11), MgII (Col. 12) and CIV (Col. 13) broad emission lines.

Name	z	P_{rad}	P_{e}	P_{B}	P_{p}	Γ	θ_{v}	$L_{\text{disk,fit}}$	$L_{\text{disk,line}}$	$M_{\text{H}\beta}$	M_{MgII}	M_{CIV}
[1]	[2]	[3]	[4]	[5]	[6]	[7]	[8]	[9]	[10]	[11]	[12]	[13]
0507-6104	1.089	45.22	44.82	45.14	47.11	12.0	3.0	45.83	45.86	—	7.74	—
0509+1011	0.621	44.66	43.88	44.64	45.52	12.0	3.0	45.26	45.35	7.03	7.52	—
0516-6207	1.300	45.52	44.34	45.04	46.03	12.0	3.0	45.73	45.74	—	7.93	7.52
0526-4830	1.300	45.45	44.54	45.09	46.69	14.0	3.0	45.78	45.87	—	9.15	7.46
0532+0732	1.254	46.02	44.95	45.26	46.94	14.0	3.0	45.95	45.86	—	7.43	—
0533+4822	1.160	45.68	44.32	46.08	46.38	13.0	3.0	46.30	46.26	—	9.25	—
0533-8324	0.784	44.66	44.06	44.04	46.02	12.0	3.0	44.73	44.73	—	7.40	—
0541-0541	0.838	45.32	44.51	45.33	46.87	13.0	3.0	46.02	46.06	—	7.74	—
0601-7036	2.409	46.28	45.27	45.06	46.32	14.0	3.0	45.78	45.69	—	—	7.36
0607-0834	0.870	45.32	44.45	45.54	46.79	12.0	3.0	46.23	46.33	7.63	9.02	—
0608-1520	1.094	45.42	44.54	44.86	46.75	14.0	3.0	45.56	45.51	—	7.09	—
0609-0615	2.219	46.60	44.87	45.82	47.26	16.0	3.0	46.52	46.53	—	—	7.89
0625-5438	2.051	46.58	44.50	45.57	47.30	15.0	3.0	46.56	46.21	—	7.40	9.07
0645+6024	0.832	45.00	44.18	45.63	46.54	12.0	3.0	46.02	46.09	9.09	9.56	—
0654+5042	1.253	45.37	44.22	45.18	45.98	12.0	3.0	44.98	44.97	—	7.86	7.79
0654+4514	0.928	45.43	44.62	44.67	46.35	12.0	3.0	45.26	45.25	—	7.17	—
0713+1935	0.540	44.39	43.59	44.38	45.09	12.0	2.4	44.78	44.93	7.33	7.91	—
0721+0406	0.665	45.23	43.96	45.87	46.07	13.0	4.0	46.26	46.33	7.49	9.12	—
0723+2859	0.966	44.74	43.66	45.38	45.53	12.0	3.0	45.77	45.75	—	7.40	—
0725+1425	1.038	45.80	44.60	45.26	46.93	14.0	3.0	45.95	45.95	—	7.31	—
0746+2549	2.979	47.35	46.00	45.78	48.40	16.0	3.0	46.48	46.31	—	—	9.23
0805+6144	3.033	47.18	45.85	45.83	48.16	15.0	3.0	46.52	46.56	—	—	9.07
0825+5555	1.418	46.02	44.90	45.66	47.33	14.0	3.0	46.35	46.32	—	9.10	—
0830+2410	0.942	45.82	44.80	45.96	47.01	12.0	3.0	46.35	45.97	—	7.70	—
0840+1312	0.680	44.83	44.39	45.04	46.86	12.0	3.0	45.73	45.75	7.37	7.62	—
0847-2337	0.059	43.67	43.22	43.24	44.98	5.0	10.0	43.18	43.32	7.30	—	—
0856+2111	2.098	45.73	44.12	45.63	46.24	15.0	3.0	46.42	47.11	—	9.96	9.77
0909+0121	1.026	45.96	44.76	46.01	47.25	13.0	3.0	46.53	46.47	—	9.14	—
0910+2248	2.661	46.37	45.04	45.48	47.19	16.0	3.0	46.18	46.21	—	—	7.70
0912+4126	2.563	45.99	44.66	46.05	46.89	11.0	3.0	46.35	46.36	—	—	9.32
0920+4441	2.189	46.64	45.30	46.41	47.81	12.0	3.0	46.71	46.70	—	—	9.29
0921+6215	1.453	45.72	44.65	45.71	46.71	12.0	3.0	46.01	46.05	—	7.93	—
0923+2815	0.744	44.92	44.14	44.79	45.91	13.0	3.0	45.48	45.63	7.61	9.04	—
0923+4125	1.732	45.47	44.51	44.18	45.98	13.0	3.0	44.88	44.75	—	7.68	7.16
0926+1451	0.632	44.61	43.97	43.09	45.30	14.0	3.0	43.78	43.75	—	7.11	—
0937+5008	0.276	43.64	43.96	43.58	46.18	11.0	3.0	43.78	43.99	7.50	—	—
0941+2778	1.305	45.02	43.98	45.02	45.83	12.0	3.0	45.71	45.72	—	7.63	—
0946+1017	1.006	45.20	44.05	44.98	46.05	12.0	3.0	45.67	45.74	—	7.47	—
0948+0022	0.585	45.01	44.66	44.79	47.22	15.0	3.0	45.35	45.03	7.46	7.73	—
0949+1752	0.693	44.92	44.33	44.55	46.53	14.0	3.0	45.25	45.25	—	7.10	—
0956+2515	0.708	44.96	44.32	45.23	46.60	10.0	3.0	45.88	45.93	7.30	7.63	—
0957+5522	0.899	45.87	44.76	44.87	46.84	11.0	4.0	45.65	45.59	—	7.45	—

Table 1: **Extended Data Table 1: Relevant parameters of the blazars studied in this paper.**
Continue.

Name	z	P_{rad}	P_{e}	P_{B}	P_{p}	Γ	θ_{v}	$L_{\text{disk,fit}}$	$L_{\text{disk,line}}$	$M_{\text{H}\beta}$	M_{MgII}	M_{CIV}
[1]	[2]	[3]	[4]	[5]	[6]	[7]	[8]	[9]	[10]	[11]	[12]	[13]
1001 +2911	0.558	44.57	44.73	43.86	46.46	16.0	3.0	43.95	44.06	7.31	7.64	—
1012 +2439	1.800	45.77	44.28	44.81	46.24	11.0	3.0	46.13	45.56	—	7.73	7.86
1016 +0513	1.714	45.88	44.61	45.26	46.53	12.0	3.0	45.65	45.55	—	7.34	7.64
1018 +3542	1.228	46.46	44.92	45.66	47.29	15.0	3.0	46.35	46.34	—	9.10	—
1022 +3931	0.604	44.49	43.57	45.19	45.46	11.0	3.0	45.88	45.89	—	7.95	—
1032 +6051	1.064	45.03	44.14	44.69	46.39	14.0	3.0	45.38	45.35	—	7.75	—
1033 +4116	1.117	45.45	44.39	45.26	46.13	14.0	3.0	45.78	45.92	—	7.61	—
1033 +6051	1.401	46.04	45.11	45.09	47.31	15.0	3.0	45.71	45.66	—	9.09	—
1037 +2823	1.066	45.47	44.34	45.34	46.28	12.0	3.0	46.03	45.95	—	7.99	—
1043 +2408	0.559	44.17	43.88	43.72	46.06	9.0	3.0	44.68	44.65	—	7.09	—
1058 +0133	0.888	45.61	44.68	45.20	46.54	14.0	3.0	45.48	45.51	—	7.37	—
1106 +2812	0.843	44.90	44.87	44.76	46.50	11.0	3.0	45.20	46.26	—	7.85	—
1112 +3446	1.956	45.89	44.60	45.59	46.52	10.0	3.0	46.28	46.13	—	7.74	7.82
1120 +0704	1.336	45.01	44.59	44.26	46.16	12.0	3.0	44.95	45.47	—	7.83	—
1124 +2336	1.549	45.45	44.48	45.25	46.35	13.0	3.0	45.83	46.05	—	7.79	—
1133 +0040	1.633	45.75	44.42	45.18	46.46	14.0	3.0	45.88	45.64	—	7.80	—
1146 +3958	1.088	45.57	44.53	45.63	46.54	12.0	3.0	46.07	46.06	—	7.93	—
1152 -0841	2.367	45.98	44.88	46.05	47.28	13.0	3.0	46.28	46.25	—	—	9.38
1154 +6022	1.120	45.59	44.52	45.26	46.53	13.0	3.0	45.95	45.97	—	7.94	—
1155 -8101	1.395	45.74	44.71	44.78	46.65	14.0	3.0	45.48	45.55	—	7.30	—
1159 +2914	0.725	45.45	44.52	44.87	46.33	12.0	3.0	45.56	45.65	7.14	7.61	—
1208 +5441	1.344	45.88	44.81	44.93	46.74	14.0	3.0	45.62	45.53	—	7.40	—
1209 +1810	0.845	44.80	43.91	44.99	45.83	12.0	3.0	45.68	45.47	7.26	7.77	—
1222 +0413	0.966	45.94	45.11	45.78	47.34	12.0	3.0	46.18	45.97	—	7.37	—
1224 +2122	0.434	45.49	44.18	45.39	46.26	13.0	3.0	46.08	46.16	7.89	7.91	—
1224 +5001	1.065	45.74	44.44	45.86	46.66	14.0	3.0	46.56	45.85	—	7.66	—
1226 +4340	2.001	46.41	44.65	45.42	47.09	16.0	3.0	46.41	46.14	—	7.64	9.01
1228 +4858	1.722	45.61	44.43	45.07	46.19	12.0	3.0	45.65	45.68	—	7.28	7.23
1239 +0443	1.761	46.81	45.48	45.14	47.58	15.0	3.0	45.83	45.83	—	7.46	7.68
1257 +3229	0.806	45.04	44.38	45.40	46.71	13.0	3.0	45.62	45.28	7.89	7.62	—
1303 -4621	1.664	45.32	44.57	44.39	46.69	13.0	3.0	45.18	45.21	—	7.95	7.21
1310 +3220	0.997	45.53	44.62	45.27	46.86	11.0	3.0	45.95	45.92	—	7.57	—
1317 +3425	1.055	44.86	44.14	45.81	46.52	11.0	3.0	46.03	46.09	—	9.14	—
1321 +2216	0.943	45.03	44.30	45.16	45.58	13.0	3.0	45.38	45.99	7.87	7.76	—
1327 +2210	1.403	45.97	45.02	45.41	47.29	13.0	3.0	46.02	45.96	—	9.25	—
1332 -1256	1.492	46.14	44.57	45.56	46.92	15.0	3.0	46.26	46.26	—	7.96	7.61
1333 +5057	1.362	45.53	44.37	44.69	46.09	15.0	3.0	45.38	45.36	—	7.95	—
1343 +5754	0.933	45.13	44.14	45.09	46.40	12.0	4.0	45.78	45.65	—	7.42	—
1344 -1723	2.506	46.19	44.84	45.64	45.94	17.0	2.4	46.03	46.02	—	—	9.12
1345 +4452	2.534	46.60	45.24	45.62	47.28	14.0	3.0	46.02	46.12	—	—	7.98
1347 -3750	1.300	45.34	44.69	45.04	47.00	12.0	3.0	45.73	45.67	—	7.95	7.62
1350 +3034	0.712	44.83	44.33	44.79	46.53	12.0	3.0	45.54	45.28	7.21	7.33	—
1357 +7643	1.585	45.57	44.84	44.48	46.84	15.0	3.0	45.18	45.20	—	7.34	7.17
1359 +5544	1.014	45.30	44.53	44.44	46.20	13.0	3.0	45.13	44.99	—	7.00	—

Table 1: **Extended Data Table 1: Relevant parameters of the blazars studied in this paper.**
Continue.

Name	z	P_{rad}	P_{e}	P_{B}	P_{p}	Γ	θ_{v}	$L_{\text{disk,fit}}$	$L_{\text{disk,line}}$	$M_{\text{H}\beta}$	M_{MgII}	M_{CIV}
[1]	[2]	[3]	[4]	[5]	[6]	[7]	[8]	[9]	[10]	[11]	[12]	[13]
1423 -7829	0.788	44.59	43.96	44.56	46.45	12.0	3.0	45.26	45.29	7.14	7.32	—
1436 +2321	1.548	45.39	44.40	45.77	46.36	11.0	3.0	46.17	45.66	—	7.12	7.50
1438 +3710	2.399	46.68	45.74	45.48	47.34	17.0	3.0	46.18	46.36	—	—	7.58
1439 +3712	1.027	45.45	44.07	45.88	46.36	14.0	3.0	46.57	46.16	—	9.08	—
1441 -1523	2.642	46.55	45.54	45.50	47.90	12.0	3.0	46.19	46.20	—	—	7.49
1443 +2501	0.939	44.64	44.12	45.03	46.72	10.0	3.0	45.26	45.28	7.42	7.84	—
1504 +1029	1.839	47.27	45.31	45.66	47.28	18.0	2.0	46.18	46.17	—	7.98	7.90
1505 +0326	0.409	44.49	43.95	44.14	45.94	14.0	3.0	44.83	44.72	—	7.41	—
1514 +4450	0.570	44.30	44.10	44.07	46.32	11.0	3.0	44.30	44.33	7.72	7.62	—
1522 +3144	1.484	45.90	44.72	44.96	47.03	12.0	3.0	45.65	45.90	—	7.92	—
1539 +2744	2.191	45.66	44.32	45.26	46.04	12.0	3.0	45.65	45.63	—	7.43	7.51
1549 +0237	0.414	44.59	43.92	45.09	46.12	11.0	3.0	45.78	45.83	7.62	7.72	—
1550 +0527	1.417	45.59	44.78	45.53	47.07	12.0	3.0	46.08	46.08	—	7.98	—
1553 +1256	1.308	45.58	43.91	46.09	45.97	12.0	3.0	46.78	46.18	—	7.64	—
1608 +1029	1.232	45.63	44.77	45.86	47.17	12.0	3.0	46.26	46.07	—	7.77	—
1613 +3412	1.400	45.29	44.41	46.43	46.96	10.0	3.0	46.73	46.46	—	9.08	—
1616 +4632	0.950	45.21	44.29	44.78	46.49	14.0	3.0	45.48	45.42	—	7.28	—
1617 -5848	1.422	46.40	44.88	46.39	47.36	15.0	3.0	47.02	47.00	—	9.81	9.01
1624 -0649	3.037	45.96	44.53	45.86	47.01	14.0	3.0	46.56	46.35	—	—	7.23
1628 -6152	2.578	46.11	45.05	45.63	47.33	12.0	3.0	46.02	46.03	—	—	7.92
1635 +3808	1.813	47.69	45.58	46.56	48.04	14.0	3.0	46.78	46.66	—	9.30	7.85
1636 +4715	0.823	45.73	44.70	44.86	47.01	15.0	3.0	45.56	45.49	7.11	7.38	—
1637 +4717	0.735	45.26	44.38	44.86	46.09	12.0	3.0	45.26	45.58	7.61	7.52	—
1639 +4705	0.860	45.53	44.21	45.26	46.33	14.0	3.0	45.95	45.97	—	7.95	—
1642 +3940	0.593	45.67	44.83	45.73	46.90	11.0	3.5	45.95	46.01	7.73	9.03	—
1703 -6212	1.747	46.37	45.06	46.03	47.22	12.0	3.0	46.72	46.31	—	7.65	7.55
1709 +4318	1.027	45.53	44.64	44.63	46.32	15.0	3.0	45.18	45.03	—	7.92	—
1734 +3857	0.975	45.40	44.27	44.91	46.00	13.0	3.0	45.30	45.01	—	7.97	—
1736 +0631	2.387	46.45	45.16	45.39	47.32	15.0	3.0	46.08	46.21	—	7.82	9.39
1802 -3940	1.319	46.24	44.78	45.66	46.78	12.0	3.0	46.18	46.11	—	7.60	7.59
1803 +0341	1.420	45.90	44.92	44.39	46.53	15.0	3.0	45.08	45.01	—	7.79	—
1818 +0903	0.354	44.11	43.43	44.19	45.01	12.0	3.0	44.88	44.93	7.30	7.50	—
1830 +0619	0.745	45.22	44.16	45.96	46.66	13.0	3.0	46.35	46.45	7.69	7.86	—
1848 +3219	0.800	45.27	44.61	45.26	46.89	13.0	3.0	45.65	45.58	7.87	7.21	—
1903 -6749	0.254	43.84	44.00	44.10	46.36	11.0	3.0	44.35	44.42	7.51	—	—
1916 -7946	0.204	44.14	43.53	43.95	45.20	13.0	3.0	44.73	44.90	7.82	—	—
1928 -0456	0.587	45.45	44.36	44.71	46.40	15.0	3.0	45.62	45.62	—	9.07	—
1954 -1123	0.683	44.80	44.04	43.90	45.46	11.0	3.0	44.48	44.37	—	6.73	—
1955 +1358	0.743	45.20	44.59	45.26	46.82	11.0	3.0	45.65	45.73	7.17	7.39	—
1959 -4246	2.178	46.03	44.61	45.86	46.62	12.0	3.0	46.16	46.13	—	7.55	9.41
2017 +0603	1.743	46.06	44.46	46.12	46.84	15.0	3.0	47.20	47.42	—	9.39	9.67
2025 -2845	0.884	45.73	44.86	44.36	46.67	13.0	3.0	45.05	45.01	—	7.34	—
2031 +1219	1.213	45.20	44.86	44.48	45.93	18.0	2.3	44.88	44.76	—	7.99	7.19
2035 +1056	0.601	44.94	44.30	44.78	46.37	12.0	3.0	45.18	45.11	7.74	7.26	—

Table 1: **Extended Data Table 1: Relevant parameters of the blazars studied in this paper.**
Continue.

Name	z	P_{rad}	P_{e}	P_{B}	P_{p}	Γ	θ_{v}	$L_{\text{disk,fit}}$	$L_{\text{disk,line}}$	$M_{\text{H}\beta}$	M_{MgII}	M_{CIV}
[1]	[2]	[3]	[4]	[5]	[6]	[7]	[8]	[9]	[10]	[11]	[12]	[13]
2110 +0809	1.580	45.21	44.19	45.65	46.43	13.0	3.0	46.05	46.08	—	7.82	—
2118 +0013	0.463	44.24	43.23	44.17	45.26	12.0	4.0	44.78	44.93	7.60	7.89	—
2121 +1901	2.180	45.98	44.74	45.09	46.97	13.0	3.0	45.78	45.26	—	—	7.75
2135 -5006	2.181	46.42	45.12	45.43	47.29	16.0	3.0	46.12	46.36	—	7.31	7.40
2139 -6732	2.009	46.56	45.46	45.18	47.79	15.0	3.0	45.88	45.77	—	7.49	7.93
2145 -3357	1.361	44.99	44.40	44.77	46.15	13.0	2.0	45.35	45.17	—	7.31	—
2157 +3127	1.448	45.73	44.69	45.38	46.62	13.0	2.4	45.73	45.74	—	7.89	—
2202 -8338	1.865	45.86	45.10	45.88	47.55	14.0	3.0	46.18	46.18	—	9.02	9.16
2212 +2355	1.125	44.93	44.26	45.09	46.94	13.0	3.0	45.78	45.78	—	7.46	—
2219 +1806	1.071	44.70	43.76	44.48	45.83	14.0	3.0	45.18	45.07	—	7.65	7.66
2229 -0832	1.560	46.32	45.05	45.83	47.17	13.0	3.0	46.48	46.45	—	7.70	7.54
2236 +2828	0.790	45.22	44.17	45.58	46.12	11.0	3.0	45.38	45.37	—	7.35	—
2237 -3921	0.297	45.06	44.62	44.26	46.87	13.0	6.0	44.78	44.87	7.77	7.95	—
2240 +4057	1.171	45.41	44.67	44.98	46.81	14.0	2.5	45.38	45.31	—	7.28	—
2315 -5018	0.808	44.66	44.38	44.80	45.76	13.0	3.0	44.65	44.62	—	7.68	—
2321 +3204	1.489	45.54	44.50	45.21	46.36	12.0	3.0	45.73	45.71	—	7.66	7.75
2327 +0940	1.841	46.42	45.32	45.79	47.76	12.0	3.0	46.48	46.20	—	7.70	9.35
2331 -2148	0.563	44.83	44.20	44.04	45.89	12.0	3.0	44.88	44.82	7.53	7.63	—
2334 +0736	0.401	44.28	43.60	45.12	45.85	12.0	3.0	45.73	45.76	7.37	—	—
2345 -1555	0.621	45.03	44.15	44.80	45.88	12.0	3.0	45.32	45.30	7.16	7.48	—
2357 +0448	1.248	45.69	44.97	44.74	47.16	15.0	3.0	45.43	46.02	—	7.41	7.45
0013 +1907	0.477	43.76	43.51	43.92	45.12	11.0	3.0	43.78	43.70	—	—	—
0203 +3042	0.761	44.71	43.85	45.87	46.19	11.0	3.0	45.73	45.75	—	—	—
0334 -4008	1.357	45.74	45.25	44.93	46.83	17.0	2.5	44.86	44.83	—	—	—
0434 -2014	0.928	44.57	43.85	44.32	45.68	11.0	3.0	44.18	44.15	—	—	—
0438 -4521	2.017	45.66	44.72	45.03	46.77	11.0	3.0	45.26	45.24	—	—	—
0516 -6207	1.300	45.65	44.57	45.25	46.70	11.0	3.0	45.48	45.43	—	—	—
0629 -2001	1.724	45.85	44.71	45.33	46.55	11.0	3.0	45.13	45.05	—	—	—
0831 +0429	0.174	43.77	43.68	43.14	44.68	10.0	3.0	43.65	43.62	—	—	—
1117 +2013	0.138	43.30	42.28	44.58	43.10	18.0	2.5	42.95	42.83	—	—	—
1125 -3559	0.284	43.50	43.02	44.29	44.27	15.0	3.0	44.43	44.34	—	—	—
1203 +6030	0.065	42.65	42.02	44.45	43.46	15.0	3.0	43.00	43.00	—	—	—
1221 +2814	0.103	43.36	43.32	43.05	43.78	10.0	3.0	43.08	43.11	—	—	—
1221 +3010	0.184	43.77	43.02	43.28	43.23	10.0	3.0	43.08	43.05	—	—	—
1420 +5422	0.153	44.00	43.89	43.33	44.60	10.0	4.0	43.26	43.20	—	—	—
1534 +3720	0.144	43.38	42.99	43.42	43.12	11.0	5.0	42.78	42.72	—	—	—
1540 +1438	0.606	44.30	44.23	44.46	45.97	10.0	3.0	44.56	44.57	—	—	—
1755 -6423	1.255	45.22	44.64	45.25	46.83	10.0	3.0	45.18	45.16	—	—	—
1824 +5651	0.664	45.18	44.58	44.91	46.67	10.0	3.0	44.91	44.91	—	—	—
2015 +3709	0.859	46.13	45.17	45.13	47.37	12.0	3.0	45.65	45.18	—	—	—
2152 +1735	0.874	44.67	44.10	44.79	44.90	10.0	3.0	45.18	45.15	—	—	—
2206 -0029	1.053	44.72	44.51	44.61	46.24	11.0	3.0	44.83	44.80	—	—	—
2206 +6500	1.121	46.01	44.74	45.64	47.24	15.0	3.0	46.62	46.67	—	—	—
2236 +2828	0.790	45.15	44.58	45.32	46.16	10.5	3.0	45.62	45.64	—	—	—
2247 -0002	0.949	44.69	44.30	44.61	45.45	11.0	3.0	45.13	45.10	—	—	—
2315 -5018	0.811	44.65	44.00	44.68	45.68	12.0	3.0	44.68	44.62	—	—	—
2353 -3034	0.737	44.35	43.56	44.56	45.20	10.0	3.0	44.68	44.63	—	—	—

Table 1: **Extended Data Table 1: Relevant parameters of the blazars studied in this paper.** *Continue.* The bottom part of this table refer to BL Lac objects.